Extracellular Space Attenuates the Effect of Gap Junctional Remodeling on Wave Propagation: A Computational Study

Candido Cabo[†‡*] and Penelope A. Boyden[‡]

[†]Department of Computer Systems, New York City College of Technology and Graduate Center, City University of New York, New York, New York; and [‡]Department of Pharmacology, College of Physicians and Surgeons, Columbia University, New York, New York

ABSTRACT   Ionic channels and gap junctions are remodeled in cells from the 5-day epicardial border zone (EBZ) of the healing canine infarct. The main objective of the study was to determine the effect of gap junctional conductance (Gj) remodeling and Cx43 redistribution to the lateral membrane on conduction velocity (θ) and anisotropic ratio, and how gap junctional remodeling is modulated by the extracellular space. We first implemented subcellular monodomain and two-domain computer models of normal epicardium (NZ) to understand how extracellular space modulates the relationship between Gj and θ in NZ. We found that the extracellular space flattens the Gj-θ relationship, thus θ becomes less sensitive to changes in Gj. We then investigated the functional consequences of Gj remodeling and Cx43 distribution in subcellular computer models of cells of the outer pathway (IZo) and central pathway (IZc) of reentrant circuits. In IZo cells, side-to-side (transverse) Gj is 10% the value in NZ cells. Such Gj remodeling causes a 45% decrease in transverse θ (θ_T). Inclusion of an extracellular space reduces the decrease in θ_T to 31%. In IZc cells, Cx43 redistribution along the lateral membrane results in a 29% increase in θ_T. That increase in θ_T is a consequence of the decrease in access resistance to the Cx43 plaques that occur with the Cx43 redistribution. Extracellular space reduces the increase in θ_T to 10%. In conclusion: 1), The extracellular space included in normal epicardial simulations flattens the Gj-θ relationship with θ becoming less sensitive to changes in Gj. 2), The extracellular space attenuates the effects of gap junction epicardial border zone remodeling (i.e., Gj reduction and Cx43 lateralization) on θ_T.

INTRODUCTION

Gap junctional proteins connect the cytoplasm of adjacent cells and provide an intracellular pathway for the flow of local circuit currents that result in the propagation of the action potential in cardiac tissue (1). Cell-to-cell conductance (Gj) in combination with the resistance of the cytoplasm and the extracellular space are important (but not the only) factors in determining conduction velocity (θ) and anisotropy (ANR) in cardiac tissue (1).

Five days after ligation of the left anterior descending coronary artery (LAD), sustained ventricular tachycardias can be initiated by electrical stimulation in the epicardial border zone (EBZ) of canine infarcted hearts. The reentrant tachycardias have a figure-of-eight pattern of activation, with a central (IZc) and an outer pathway (IZo). There are major functional changes (remodeling) in sarcolemmal ion currents (e.g., I_{Na}, $I_{Ca,L}$) (2), Gj and Cx43 distribution (3,4) in the EBZ. In the IZo, side-to-side (transverse) Gj between cell pairs is reduced by 90% but transverse conduction velocity (θ_T) is reduced only by 39% with respect to normal cells (4). This amount is about half the reduction expected from theoretical considerations in continuous myocardium. The anisotropic ratio− (ANR) in IZo is 2.1, which is only a modest increase over the value in normal epicardium, 1.6 (4). The mechanisms by which major Gj remodeling in

IZo cells results in relatively modest functional changes in θ_T and ANR are not completely understood. Previous computer simulations of normal myocardium (5–7) suggest that the Gj-θ relationship is not very steep at least for certain ranges of Gj. However, those studies did not investigate how other structural factors important for propagation in the in situ heart, like the resistance of the extracellular space, may modulate the relationship between Gj and θ. In IZc cells, side-to-side Gj between cell pairs is about the same as between normal (NZ) cell pairs, but Cx43 protein redistributes to the lateral membrane (Cx43 lateralization) (4). The functional consequences of Cx43 lateralization in cells surviving in the infarcted myocardium and their modulation of function by the extracellular space have not been completely characterized.

To quantify the effects of Gj remodeling, Cx43 redistribution to the lateral membrane, and the extracellular space on θ and ANR in the infarcted canine heart, we implemented a subcellular computer model of the canine EBZ, inspired by the subcellular computer models pioneered by Spach et al. for normal tissue (8), and that have been used more recently to understand normal and abnormal microscopic conduction (9,10). In the model we incorporated the detailed descriptions of sarcolemmal currents for normal (NZ) and border zone epicardial cells (IZc, IZo) that we previously developed (2). We hypothesized that the extracellular space flattens the Gj-θ relationship and reduces the impact of Gj remodeling and Cx43 distribution on propagation and anisotropy.

METHODS

Cell architecture

To study the effect of gap junction remodeling (i.e., changes in cell-to-cell Gj and Cx43 spatial distribution (3,4)) on propagation and anisotropy, we used the cell architecture shown in Fig. 1. In this model all cells have the same length (130 μm) and width (26 μm), to prevent the effects of heterogeneity of cell size and shape on propagation (11). Each cell is connected to six neighboring cells, cells overlap in the longitudinal and the transverse directions, and gap junctions are located within 10–20% of the cell ends at the intercalated disks (IDs), all characteristic of ventricular myocardium architecture (12,13). Table 1 compares different cell parameters in experiments and the computer model. Except at the sites where gap junctions are present (Fig. 1), there is no resistive connection between the cytoplasm of adjacent cells.

Cell-to-cell Gj

Ventricular myocytes are electrically connected by IDs, which range in size from 40 to 100 μm^2 (12). IDs contain many gap junction plaques (1.5–6.6 μm^2) located in the plicate and interplicate regions of the disk. Most experimental evidence demonstrating Gj remodeling occurring in the infarcted heart is based on end-to-end and side-to-side cell-to-cell conductance measurements in cell pairs isolated from the EBZ (3,4). Since cell-to-cell Gj is a global measurement of the conductance of many (plicate and interplicate) gap junction plaques (12), we represented electrical connections between cells at the level of IDs (Fig. 1), assuming that modeling individual gap junction plaques is not necessary for the purpose of our study. Our experimental measurements of Gj ~ 0.1 μS in normal canine ventricular epicardium are within the range of reported macroscopic measurements of Gj, which vary widely from 0.026 to 3.078 μS (3). Jongsma and Wilders (6) estimate Gj to be between 3 and 12 μS based on morphometric data and computer simulations. Here, for each model, we simulate propagation for a range of Gj values from 0.1 to 7 μS that covers the range of reported and estimated values of Gj. Gj between cell pairs isolated from the outer pathway (IZo) of figure-of-eight EBZ reentrant circuits is normal for end-to-end coupled pairs, but it is reduced to ~10% normal value for side-to-side coupled cell pairs (3). Gj between cell pairs of the central pathway of EBZ figure-of-eight reentrant circuits (IZc) is normal for end-to-end and side-to-side pairs, but Cx43 redistributes to lateral cell membranes (4). That redistribution of Cx43 is modeled by redistributing of gap junctions to sites along the lateral membrane, while keeping the same total side-to-side Gj. The ratio of side-to-side and end-to-end conductances measured experimentally is ~25% (3). If all gap junction sites (small segments in Fig. 1) have the same conductance (gj) regardless their longitudinal or transverse orientation, then the ratio of the average side-to-side conductance (2 gj) and the average end-to-end conductance (1.5 gj) is about the same as that measured experimentally in normal tissue (3). The average Gj between cells, including end-to-end and side-to-side connections, is 1.67 gj.

Ionic models

The ionic cell action potential models of normal (NZ), common central pathway (IZc), and outer pathway (IZo) cells used in different simulations in this article have been described (2,16,17). All major depolarizing and
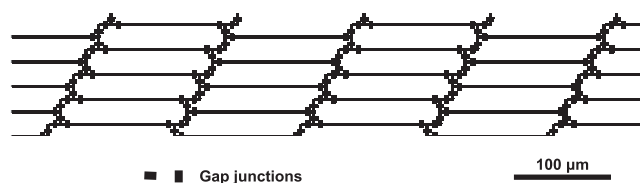

- ■ ▮ Gap junctions

100 μm

FIGURE 1 Myocardial architecture.

repolarizing currents are affected by the remodeling that occurs after myocardial infarction (2). In general, ionic channel remodeling causes a reduction in channel function. Consequently, conduction velocity in cells of the EBZ (IZo, IZc) is decreased and the refractory period is increased when compared to normal epicardial cells (NZ) (2). Remodeling of the EBZ is heterogeneous: sodium and L-type calcium currents in central pathway cells (IZc) show a reduction in function with respect to outer pathway cells (IZo).

Numerical methods

We performed simulations first with a monodomain model and then with a two-domain model that incorporates a restricted extracellular space. For the monodomain simulations, the governing equation can be expressed as: $\nabla \times (D \ \nabla V_m) = (I_{ion}/C_m) + \partial_t V_m$, where D is the diffusion coefficient, V_m is the transmembrane potential, I_{ion} is the ionic current (μA/cm^2), and C_m is the specific capacitance (1 μF/cm^2). Neumann (nonflow) boundary conditions were used. The diffusion coefficient, D, can be expressed as $1/(S_v R_i C_m)$. R_i, the resistivity of the intracellular space (i.e., cytoplasm), was 250 Ωcm (11); the surface/volume ratio, S_v, was 2000 cm^{-1}. Cells were discretized with a space step of 13 μm in both longitudinal and transverse directions. The governing equation was integrated using the semi-implicit Crank-Nicholson method with a time step of 0.5 μs (18). In the monodomain simulations, the extracellular space was considered unbounded and therefore the extracellular resistance zero.

In a second set of simulations a continuous extracellular (interstitial) space was added to the model, while keeping the same discontinuous intracellular space described above. We will refer to this model as a two-domain model (19). The two-domain model is related but not identical to the classical bi-domain model, which is continuous both in the intra- and extracellular spaces, and for which, a single point in space has associated an intracellular and extracellular potential (20). The space and time discretization steps were the same as for the monodomain model above. For the extracellular resistivities, we used 0.854 KΩcm, and 1.250 KΩcm for the longitudinal and transverse direction, respectively, values obtained in in vivo normal canine left ventricle by Roberts and Scher (21).

Conduction velocity and anisotropy

We ran all simulations in preparations that had a size of 6.5 mm in the longitudinal direction (50 cells, 500 nodes) and 3.25 mm (125 cells, 250 nodes) in the direction transverse to the fiber orientation. To initiate a propagating wave, flat wavefronts were initiated at the boundary of the preparation by electrical stimulation (2× diastolic threshold). To avoid contamination by the electrical stimulus and the preparation boundaries, conduction velocity was calculated in the center of the preparation in an area of 390 μm (three cells long) by 130 μm (five cells wide). Velocity was calculated as the reciprocal of the regression coefficient of the activation times over space in the direction of propagation. The ANR was calculated as the ratio of the longitudinal (θ_L) and the transverse (θ_T) conduction velocity.

Transverse space constant and effective intracellular resistivity

Transverse space constants were calculated from the spatial decay of V_m, in the direction transverse to the fiber orientation, five membrane time constants (40 ms) after one end of the preparation aligned with the fiber orientation was clamped at −65 mV. The effective transverse intracellular resistivity (R_{iT}, which combines the cytoplasmic and gap junctional resistance) for a given structure of the intracellular space (i.e., Gj conductance and gap junction distribution) was calculated from the transverse space constants of the monodomain model (λ_{monoT}) and the corresponding two-domain model (λ_{twoT}). From $\lambda_{monoT} = (K/R_{iT})^{0.5}$ and $\lambda_{twoT} = (K/(R_{iT} + R_{eT}))^{0.5}$, where K is a constant that depends on the membrane resistance and S_v, and R_{eT} is the extracellular resistivity in the transverse direction which is known (1.250 KΩcm in normal canine ventricle, see above) we can derive $R_{iT} = R_{eT}/((\lambda_{monoT}/\lambda_{twoT})^2 - 1)$.

TABLE 1   Cell parameters

	Computer model	Experiments (NZ cells)	Experiments (EBZ cells)	References
Cell length	130 μm	129 μm	135 μm	(14)
Cell width	26 μm	26 μm	28 μm	(14)
Cell surface area	6760 μm^2	5549 μm^2 7700 μm^2	5142 μm^2 9200 μm^2	(3,14)
Cell volume	33,800 μm^3	39,570 μm^3	36,887 μm^3	(3)
Surface/volume ratio	0.2 μm^{-1}	0.3 μm^{-1} 0.14 μm^{-1}	0.14 μm^{-1}	(3,15)
Neighboring cells	6	9	NA	(12) (in 3D myocardium)

Differences between the experimental NZ and EBZ cell parameters are not statistically significant.

Calculation of junctional resistance in cell pairs

We calculated the junctional resistance between cell pairs in an unbounded extracellular space for different distributions of Cx43 plaques using a monodomain model. The two cells (each cell had a length of 100 μm and a width of 20 μm) were discretized with a space step of 1 μm (total number of nodes was 100 × 40). The governing equation for the monodomain model (see above Numerical methods) was integrated with a time step of 1 ps. Intracellular currents were applied at one or two nodes in cell1 and at one or two nodes in cell2 to maintain the clamped nodes in cell1 at 10 mV and the clamped nodes in cell2 at 0 mV. The junctional resistance, R_{junct}, can then be calculated as the quotient of the voltage at which the node(s) on cell1

are clamped (10 mV) over the current necessary to keep the clamped node(s) in cell2 at 0 mV (3). Isopotential lines were drawn every 0.5 mV.

RESULTS

Effect of the extracellular space on subcellular propagation in normal epicardial cells

Fig. 2 shows the values of θ_L (Fig. 2 A), θ_T (Fig. 2 B), and ANR (Fig. 2 C), as a function of cell-to-cell Gj in a model of normal canine left ventricular epicardium (NZ model)
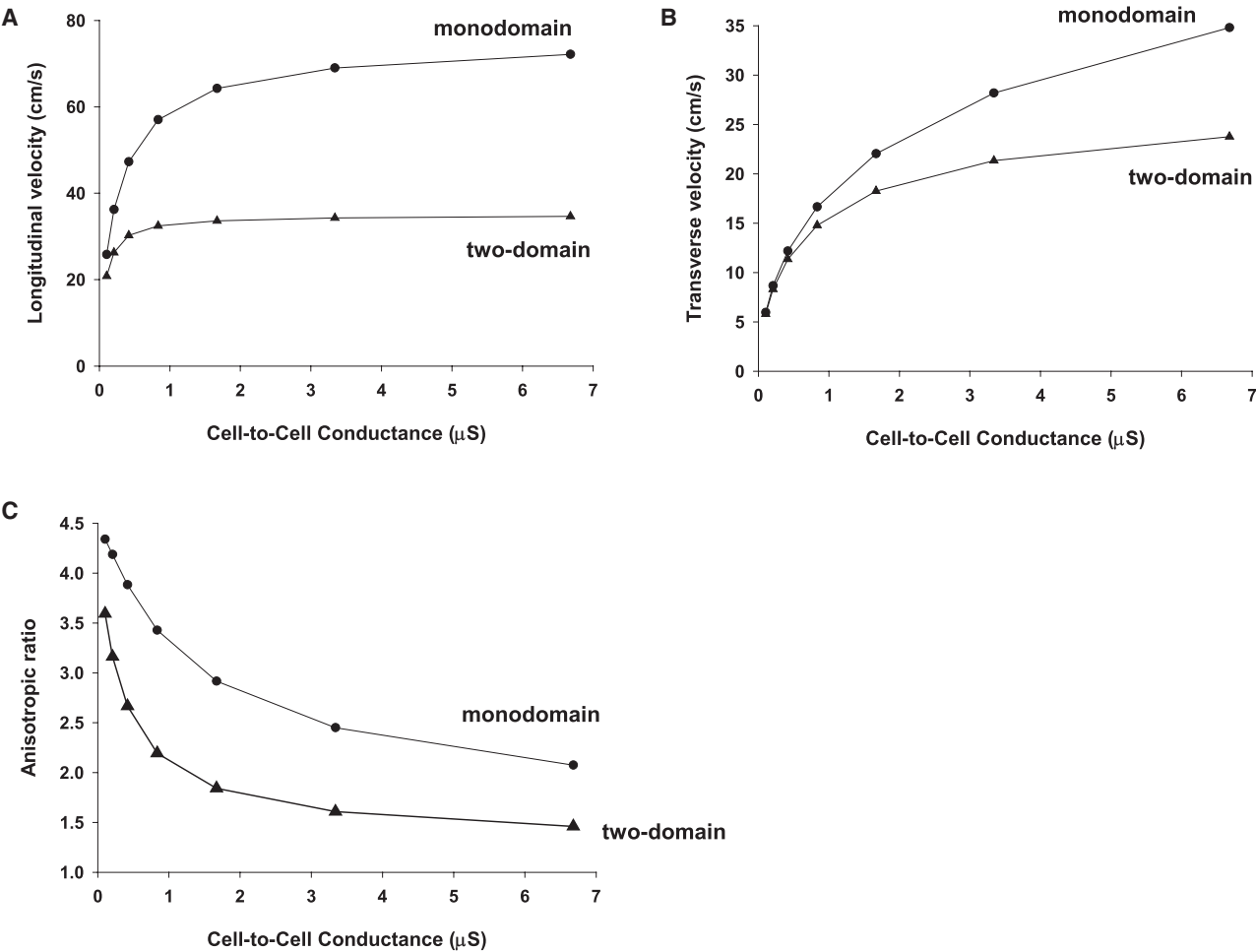

FIGURE 2   Relationship between cell-to-cell conductance (Gj) and longitudinal conduction velocity (A), transverse conduction velocity (B), and ANR (C), for a two-dimensional monodomain and two-domain model of normal (NZ) epicardial cells.

for a monodomain and two-domain model. θ_L and θ_T decrease with decreasing cell-to-cell coupling (Fig. 2, *A* and *B*) whereas ANR increases (Fig. 2 *C*), indicating that θ_T is more sensitive than θ_L to changes in cell coupling (6). The mechanism (of the greater sensitivity of θ_T to changes in cell coupling) can be explained by the relative contribution of junctional and cytoplasmic delay to total cell delay and the dependence of those delays on Gj (Supporting Material, Fig. S1). Including the extracellular space decreases both θ_L and θ_T for all values of Gj because there is additional resistance to the flow of local circuit currents (Fig. 2, *A* and *B*, two-domain) as demonstrated experimentally by Fleischhauer et al. (22). The presence of an extracellular space in the two-domain model flattens the Gj-θ relationship compared to the monodomain model (Fig. 2, *A* and *B*) and therefore makes θ_L and θ_T less sensitive to changes in Gj. The extracellular space also reduces ANR (compared to the monodomain model) for all values of Gj (Fig. 2 *C*), because θ_L is more affected than θ_T by a restricted extracellular space. Activation maps and junctional and cytoplasmic delays during propagation in the two-domain model of normal epicardium (NZ) are shown in Fig. S2.

Effect of reduced side-to-side conductance on propagation in the outer pathway of figure-of-eight reentrant circuits

Gj between cell pairs isolated from the outer pathway of figure-of-eight EBZ reentrant circuits (IZo) is normal for end-to-end coupled pairs, but it is reduced to ~10% the normal value for side-to-side coupled cell pairs (3). To quantify the effect of Gj remodeling on conduction in the outer pathway, we compared θ_L, θ_T, and ANR in a model without Gj remodeling (i.e., 100% Gj) and in a model incorporating the Gj remodeling measured experimentally (i.e., side-to-side Gj reduced to 10%). End-to-end cell pair coupling was the same in both models, which also had the same membrane dynamics (IZo). Fig. 3 *A* shows the effects of Gj remodeling on propagation in the monodomain model. Note that θ_L was not affected by Gj remodeling (solid and dashed lines in Fig. 3 *A*, *left*) but remodeling of Gj caused a reduction of θ_T (45% for Gj = 6.7 μS) that resulted in an increase in ANR (181% for Gj = 6.7 μS) (Fig. 3 *A*, *center* and *right*). Fig. 3 *B* shows the effects of Gj remodeling on propagation in the two-domain model. As in the monodomain model, θ_L was not affected by Gj remodeling
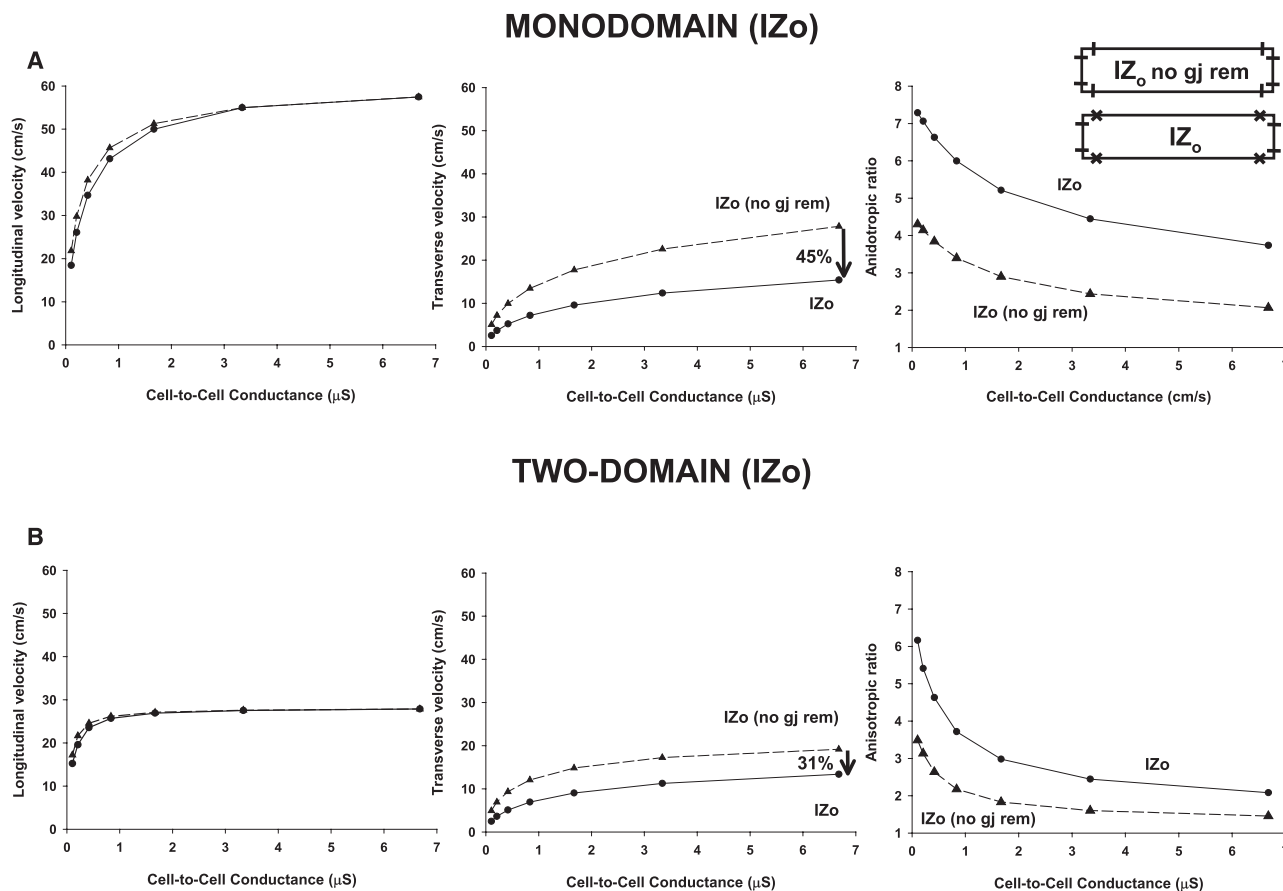

FIGURE 3   Effect of reduced side-to-side conductance (Gj remodeling) on propagation in the outer pathway of figure-of-eight reentrant circuits (IZo cells). Comparison of longitudinal velocity (*left*), transverse velocity (*center*), and ANR (*right*) between a nonremodeled IZo substrate (*dashed line*) and a remodeled IZo substrate (*solid line*) in a monodomain (*A*) and a two-domain model (*B*). (See text for explanation.)

(Fig. 3 B, left). The effect of Gj remodeling on θ_T (31% reduction for Gj = 6.7 μS) and ANR (140% increase for Gj = 6.7 μS) was reduced in the two-domain model (Fig. 3 B, center, right) when compared to the monodomain model (Fig. 3 A, center, right) indicating that the presence of an extracellular space attenuates the functional effects of Gj remodeling in IZo cells. Note that the attenuating effect of the extracellular space is more pronounced at values of Gj > 1 μS, consistent with the modest effect of the extracellular space on transverse propagation for Gj < 1 μS (Fig. 2).

Effect of redistribution of Cx43 to the lateral membrane on propagation in the central common pathway of figure-of-eight reentrant circuits

In cells from the central pathway of EBZ figure-of-eight reentrant circuits (IZc), Cx43 redistributes to lateral cell membranes (4). In this section we determined the effect that redistribution of Cx43 (mimicked by redistribution of gap junctions) to sites along the lateral membrane (with the same total side-to-side Gj) would have on θ and ANR. We compared θ_L, θ_T, and ANR in two models of the central pathway, one with normal Cx43 distribution located at the IDs and another with Cx43 redistributed to the lateral membrane (Fig. 4, upper right inset). Both models had the same membrane dynamics (IZc) and the same total end-to-end and the same total side-to-side (lateral) Gj. We also assumed that Cx43 at the lateral membrane formed gap junctions between neighboring cells. Fig. 4 A shows the effects of Cx43 lateralization on propagation in the monodomain model. First, there were no major changes in θ_L (Fig. 4 A, left). Second, Cx43 redistribution resulted in an increase in θ_T and a decrease in ANR (Fig. 4 A, center, right). Fig. 4 B shows the effects of Cx43 lateralization on propagation in the two-domain model. The increase in θ_T (Fig. 4 B, center) and the decrease in ANR (Fig. 4 B, right) were smaller in the two-domain model indicating that the presence of an extracellular space attenuates the effects of Cx43 lateralization on propagation in a substrate of IZc cells.

Mechanism of attenuation of the effects of Gj remodeling and Cx43 lateralization on θ_T by the extracellular space

Gap junction remodeling in a substrate of IZo or IZc cells (Figs. 3 and 4) changes the passive tissue structure (i.e., it changes the
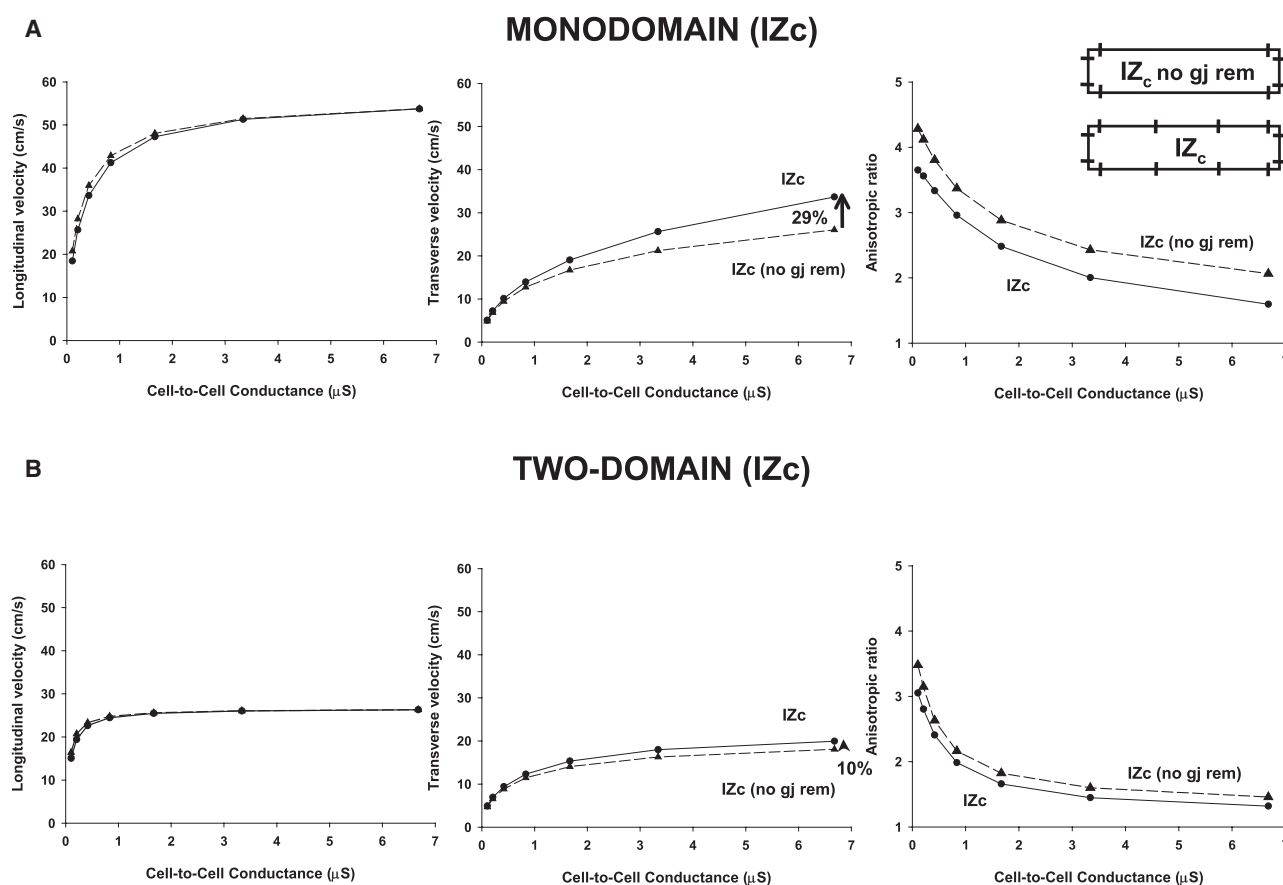

FIGURE 4 Effect of redistribution of Cx43 to the lateral membrane (Cx43 lateralization) on propagation in the central pathway of figure-of-eight reentrant circuits (IZc cells). Comparison of longitudinal velocity (left), transverse velocity (center), and ANR (right) between a nonremodeled IZc substrate (dashed line) and a remodeled IZc substrate (solid line) in a monodomain (A) and a two-domain model (B). (See text for explanation.)

effective transverse intracellular resistivity). Therefore, the mechanisms involved in the attenuation of the effects of Gj remodeling and Cx43 lateralization by the extracellular space on θ_T can be interpreted in terms of transverse space constants (λ). For example, Fig. 5 A (top) shows the spatial decay in V_m, in the transverse direction, in an IZo substrate, when cell-to-cell Gj = 6.7 μS, for the four models in Fig. 3: 1), Gj remodeling (10% Gj), monodomain; 2), no Gj remodeling (100% Gj) monodomain; 3), Gj remodeling (10%) two-domain; and 4), no Gj remodeling (100% Gj) two-domain. As expected, the two-domain models have smaller λ-values (which were estimated from the spatial decay of V_m) than the corresponding monodomain models because the extracellular space adds additional resistance to current flow. Fig. 5 A (bottom) shows transverse λ-values versus transverse resistivity (R) for the four models (see Methods). The data points in Fig. 5 A (bottom) were fitted by $\lambda = (K/R)^{0.5}$ (with $K = 4$ Ω cm^3), which is the classical expression for λ derived from the cable equations.

The difference between the λ-values for the 100% Gj and 10% Gj monodomain models (large double arrow in Fig. 5 A, bottom) is larger than the difference of λ-values for the 100% Gj and 10% Gj two-domain models (small double arrow in Fig. 5 A, bottom). The additional resistance to current flow that results from the presence of the extracellular space in the two-domain models shifts the values of the 100% Gj and 10% Gj monodomain models along the curve to a region of larger R, where the λ versus R curve is flatter (Fig. 5 A, bottom). Transverse λ-values are directly proportional to θ_T (C. Cabo and P. A. Boyden, unpublished). Therefore, the reduction of the impact of Gj remodeling (i.e., a change in effective transverse intracellular resistivity) on θ_T in IZo cells by the extracellular space is a consequence of the reciprocal square-root decay of λ with R that flattens as R grows.

A similar mechanism explains the attenuation of the effects Cx43 lateralization on θ_T by the extracellular space in IZc cells (Fig. 4). Fig. 5 B (top) shows the spatial decay
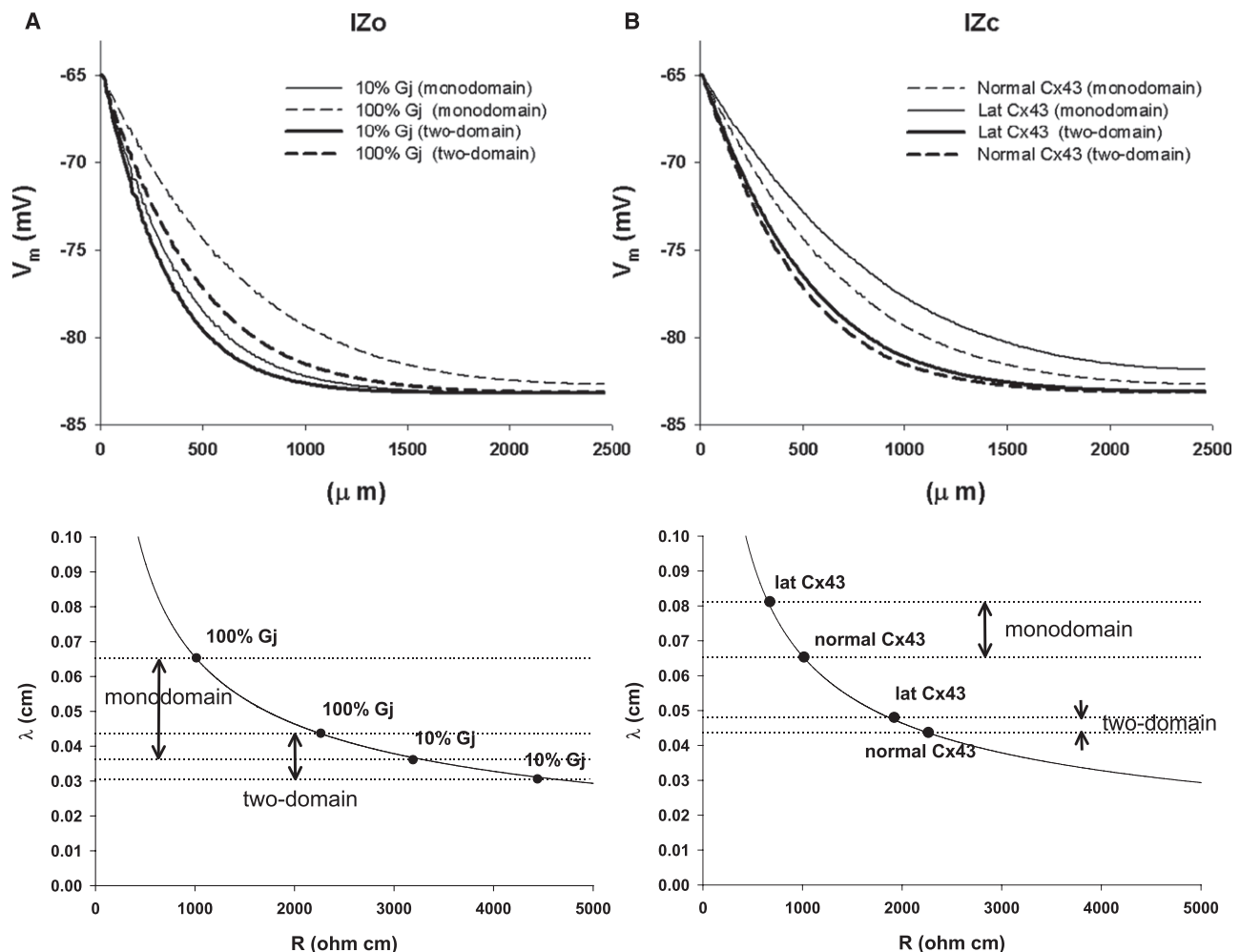

FIGURE 5 (A) Top: Plot of Vm decay in the four IZo models in Fig. 3 (Gj = 6.7 μs) to calculate the transverse space constant. Bottom: Plot of the transverse space constants versus transverse resistivity for the four IZo models in Fig. 3 (Gj = 6.7 μs). (B) Top: Plot of Vm decay in the four IZc models in Fig. 4 (Gj = 6.7 μs) to calculate the transverse space constant. Bottom: Plot of the transverse space constants versus transverse resistivity for the four IZc models in Fig. 4 (Gj = 6.7 μs). See text for explanation.

in V_m, in the transverse direction, in an IZc substrate, when cell-to-cell Gj = 6.7 μS for the four models in Fig. 4: 1), normal Cx43, monodomain; 2), lateralized Cx43 monodomain; 3), normal Cx43 two-domain; and 4), lateralized Cx43 two domain. Fig. 5 B (bottom) shows transverse λ versus R for the four models. The best fit for the four points is the same as before indicating that the subthreshold response of the IZo and IZc membranes is the same (both have a membrane resistance of 8028 Ω cm^2). As it was the case for IZo cells, the difference between the λ-values for the "lat Cx43" and "normal Cx43" monodomain models (large double arrow in Fig. 5 B, bottom) is larger than the difference of λ-values for the "lat Cx43" and "normal Cx43" two-domain models (small double arrow in Fig. 5 B, bottom). Therefore, as above, the reduction of the impact of Cx43 lateralization (i.e., a change in effective transverse intracellular resistivity) on θ_T in IZc cells by the extracellular space is a consequence of the reciprocal square-root decay of λ with R.

Mechanism of the increase in θ_T with Cx43 lateralization: access resistance to gap junction plaques

The simulations in Fig. 4 showed that when a given amount of gap junction channel protein is distributed along the lateral membrane, θ_T is larger than when that same number of chan-

nels is concentrated at the IDs. To investigate the mechanism of that increase, we calculated the side-to-side junctional resistance, R_{junct}, between two IZc cells for three different Cx43 distribution structures (Fig. 6 A). In Fig. 6 A-1, there is only one gap junction plaque connecting cell1 and cell2 with resistance R_{plaque}. R_{junct} is the sum of the resistance of the gap junction plaque (R_{plaque}) and the access resistance to the plaque (R_{acc1}). The access resistance is the resistance along the path of the current (i.e., orthogonal to the isopotential lines shown in cell1 and cell2) from site A to the gap junction plaque connecting cell1 and cell2, and from the plaque to site B (23–25). Fig. 6 B (solid circles) shows R_{junct} as a function of R_{plaque} for structure 1 in Fig. 6 A. The value of the access resistance (R_{acc1} = 1.05 MΩ) does not change with R_{plaque}, but the relative contribution of the access resistance to R_{junct} decreases as the value of R_{plaque} increases. For example for R_{plaque} = 0.25 MΩ, R_{acc1} is 81% of R_{junct}; when R_{plaque} = 4 MΩ, R_{acc1} is 20% of R_{junct}. In Fig. 6 A-2 instead of having only one gap junction plaque connecting cell1 and cell2, the plaque was divided in two plaques, separated 40 μm, each having half of the conductance (or double the resistance) of the plaque in Fig. 6 A-1 to mimic Cx43 lateralization. The access resistance is reduced by 14% from 1.05 MΩ to 0.89 MΩ (Fig. 6 B, open circles, R_{acc2}). If in addition to cells being connected by two gap junction plaques, intracellular currents are applied at two sites on each cell (A
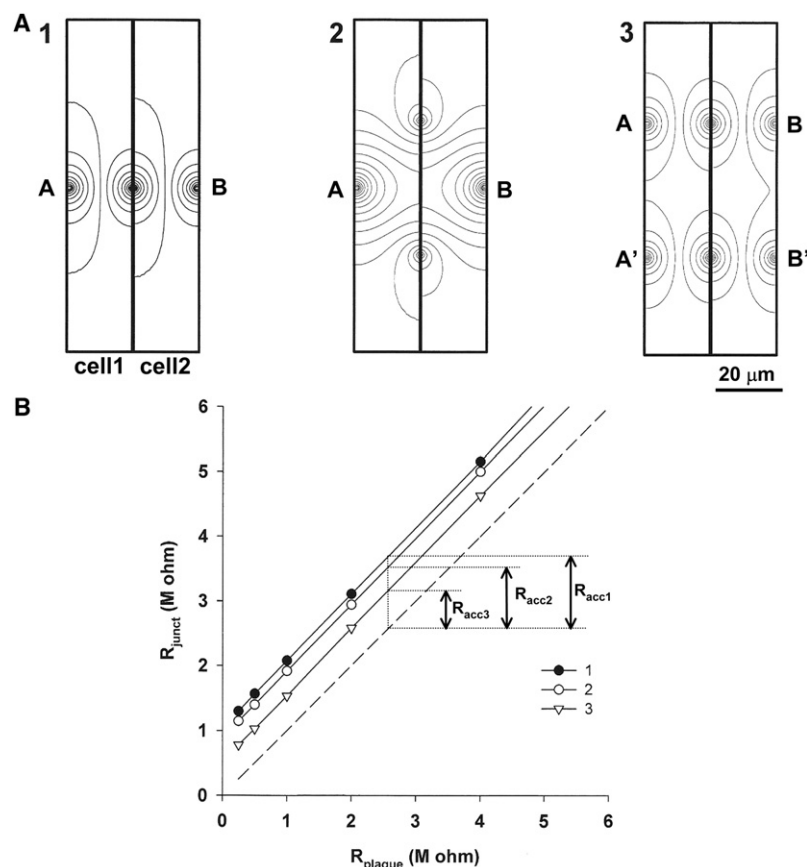

FIGURE 6 Junctional and access resistance between cell pairs coupled side-to-side. (A) Isopotential lines when node A (A and A′ in structure 3) in cell1 is clamped to 10 mV and node B (B and B′ in structure 3) in cell2 is clamped to 0 mV in three structures with different Cx43 plaque distributions. Isopotential lines are drawn every 0.5 mV. (B) Side-to-side junctional resistance, R_{junct}, between cell1 and cell2 for the three structures (1, 2, and 3,) in panel (A) as a function of the Cx43 plaque resistance (R_{plaque}) between cell1 and cell2. See text for explanation.

and A′ in cell1 and B and B′ in cell2), as it is shown in Fig. 6 *A-3*, the access resistance is further reduced to 0.53 MΩ (Fig. 6 *B*, *inverted open triangles*, R_{acc3}) (a 50% reduction with respect to the value for the structure in Fig. 6 *A-1*). The reduction in access resistance and consequently in total junctional resistance that occurs when a given amount of Cx43 is distributed over the lateral membrane (compare structures 1 and 3 in Fig. 6 *A*) explains the increase in θ_T with Cx43 lateralization (Fig. 4 *A*, *center*). The relative contribution of access resistance to R_{junct} (i.e., R_{acc}/R_{junct}) decreases as R_{plaque} increases (or cell-to-cell Gj decreases) (Fig. 6 *B*). Thus, at large values of R_{plaque}, different access resistances resulting from different distributions of Cx43 plaques are not expected to create large differences in R_{junct}. Those results explain the small differences in θ_T between substrates with normal and lateralized Cx43 distribution for Gj < 1 μS (Fig. 4 *A*, *center*).

DISCUSSION

In this study we have shown that the extracellular space flattens the Gj-θ relationship in a substrate of normal cells, which results in θ being less dependent on Gj. We have also demonstrated that, in a EBZ substrate of cells remodeled by myocardial infarction, the extracellular space reduces the impact of Gj remodeling and Cx43 lateralization on θ and ANR.

Effect of the extracellular space on subcellular propagation in normal epicardial cells

The electrical resistivity of the extracellular space is an important determinant of the velocity of propagation in ventricular myocardium (22,26). The results of our computer simulations are consistent with those experimental findings (Fig. 2), and further demonstrate how the extracellular space modulates the Gj-θ relationship. The effect of the extracellular space on conduction is larger at larger Gj (Fig. 2); this differential effect of the extracellular space flattens the Gj-θ relationship.

The simulations in Fig. 2 are consistent with the effects of an overall reduction of Gj on propagation (not just side-to-side Gj reduction) seen in conditional Cx43 knockout mice (27). In those transgenic mice, Gj is reduced by ~99% with respect to the values of wild-type mice in both the end-to-end and side-to-side directions (28). Still, despite that dramatic reduction in Gj, propagation is still possible: θ_L was reduced by 45% and θ_T was reduced 55%. Transverse propagation is more affected than longitudinal propagation by the decrease in Gj, and as a result ANR increased from 1.66 to 2.1 (27). Consistent with those experimental results, Fig. 2 shows that an overall reduction in Gj affects θ_T to a larger extent than θ_L resulting in an increase in ANR as Gj decreases (Fig. 2 *C*) (the mechanism is discussed in the Supporting Material). The experimental measurements of conduction velocity by Gutstein et al. (27) were done in vivo (i.e., myocardium with a restricted extracellular space). Thus we suggest that by flattening the Gj-θ relationship, the extra-

cellular space attenuates the functional effect of Gj reduction on conduction velocity.

In this study we used the extracellular resistivities measured experimentally by Roberts and Scher (21) for canine left ventricular epicardium. However, it is possible that the measurements by Roberts and Scher (21) do not accurately represent the impedance of cardiac tissue. Plonsey and Barr (29) showed that the interpretation of voltage and currents measurements depend on the assumptions about the underlying tissue structure. Recent theoretical work (30,31) on impedance measurements will likely lead to more accurate measurements of cardiac tissue resistivities.

Functional effect of Gj remodeling on propagation in the outer pathway of EBZ figure-of-eight reentrant circuits

Gj between cell pairs isolated from the outer pathway of figure-of-eight reentrant circuits is normal for end-to-end coupled pairs, but it is reduced to ~10% the normal value for side-to-side coupled cell pairs (3). From theoretical considerations in continuous myocardium, it would be expected that such a reduction in Gj would cause a reduction in θ_T to ~30% the value for normal tissue and an increase in ANR to ~6 (i.e., ~3–4 times the value of normal canine epicardium). A further reduction in θ_T would be expected as a result of Na channel remodeling of the outer pathway cells (2). However, θ_T measured in the outer pathway is ~61% of the value of normal tissue and the ANR is increased from 1.6 to 2.1 (4). We propose three possible (and perhaps complementary) explanations for the less than expected change in θ_T and ANR after major changes in side-to-side Gj. When there is lateral overlap between cells (as it is in cardiac tissue), transverse propagation can still occur for very small side-to-side Gj as the wavefront zigzags through the end-to-end (longitudinal) connections that have normal Gj (C. Cabo and P. A. Boyden, unpublished). Zigzag propagation patterns have been demonstrated experimentally in infarcted tissue (32), and in computer models with structural discontinuities (10). A second possibility is that normal Gj lies in a region of the Gj-θ relationship that is not very steep. For example for Gj = 6.7 μS, if side-to-side (transverse) Gj is reduced by 90%, θ_T is reduced to ~55% that of normal myocardium in the monodomain model (Fig. 3). Finally, during propagation in the intact heart, the presence of the extracellular space could further attenuate the effect of Gj remodeling on θ_T: θ_T is reduced to ~69% the value in normal myocardium (two-domain model simulations in Fig. 3).

Functional effect of Cx43 lateralization on propagation in the central pathway of EBZ figure-of-eight reentrant circuits

Cx43 protein redistributes to the lateral membranes in cells from the central pathway of figure-of-eight reentrant circuits (4). Here we show that Cx43 lateralization increases θ_T (if

Cx43 forms functional channels in the lateral membrane) even without an increase in the total number of gap junctional channels. This is a consequence of the decrease in access resistance to the gap junction plaques when Cx43 redistributes to the lateral membrane (Fig. 6). However, as we show here, the magnitude of that increase depends on Gj and on the presence of an extracellular space. In the absence of a restricted extracellular space (for example in cell monolayers), Cx43 lateralization could increase θ_T up to 29% when Gj = 6.7 μS (Fig. 4 A, center). In a monodomain model with variable cell size, Spach et al. (11) also found that Cx43 lateralization (neonatal gap junction distribution) decreased cell-to-cell delay during transverse propagation (and therefore increased θ_T) by ~10%. However, when the extracellular space is considered, the effect of lateralization on θ_T is attenuated (a 6–10% increase) for Gj ranging from 0.4–7 μS. Therefore, we can conclude that, in intact tissue, redistribution of Cx43 protein to the lateral membrane has a small functional effect, if any, on propagation between central pathway cells. In the simulations above, we assumed that the junctions at the lateral membrane are functional. If lateralized Cx43 protein does not form junctions, or the junctions formed are nonfunctional, the functional effect of the lateralized Cx43 on propagation would be nil.

Limitations

The microscopic structure of the plicate and interplicate regions of the gap junctions is not incorporated in the model. In future studies, we plan to incorporate these two elements in our computer models. We have used values of extracellular resistivity measured in normal canine epicardium in our simulations of propagation in central and outer pathway. However, the resistance of the extracellular space may be affected by swelling and edema in 5-day-old canine infarcted hearts (33) and it may increase after ischemic episodes (34). Furthermore, it is possible that the impedance measurements by Roberts and Scher (21) do not accurately represent the resistivities of cardiac tissue (29).

SUPPORTING MATERIAL

Two figures are available at http://www.biophysj.org/biophysj/supplemental/S0006-3495(09)00476-7.

REFERENCES

1. Kleber, A. G., and Y. Rudy. 2004. Basic mechanisms of cardiac impulse propagation and associated arrhythmias. *Physiol. Rev.* 84:431–488.

2. Baba, S., W. Dun, C. Cabo, and P. A. Boyden. 2005. Remodeling in cells from different regions of the reentrant circuit during ventricular tachycardia. *Circulation.* 112:2386–2396.

3. Yao, J. A., W. Hussain, P. Patel, N. S. Peters, P. A. Boyden, et al. 2003. Remodeling of gap junctional channel function in epicardial border zone of healing canine infarcts. *Circ. Res.* 92:437–443.

4. Cabo, C., J. A. Yao, P. A. Boyden, S. Chen, W. Hussain, et al. 2006. Heterogeneous gap junction remodeling in reentrant circuits in the epicardial border zone of the healing canine infarct. *Cardiovasc. Res.* 72:241–249.

5. Shaw, R., and Y. Rudy. 1997. Ionic mechanism of propagation in cardiac tissue: roles of the sodium and L type currents during reduced excitability and decreased gap junction coupling. *Circ. Res.* 81:727–741.

6. Jongsma, H. J., and R. Wilders. 2000. Gap junctions in cardiovascular disease. *Circ. Res.* 86:1193–1197.

7. Thomas, S. P., J. P. Kucera, L. Bircher-Lehmann, Y. Rudy, J. E. Saffitz, et al. 2003. Impulse propagation in synthetic strands of neonatal cardiac myocytes with genetically reduced levels of connexin 43. *Circ. Res.* 92:1209–1216.

8. Spach, M. S., and J. F. Heidlage. 1995. The stochastic nature of cardiac propagation at a microscopic level. Electrical description of myocardial architecture and its application to conduction. *Circ. Res.* 76:366–380.

9. Spach, M. S., J. F. Heidlage, P. C. Dolber, and R. C. Barr. 2007. Mechanism of origin of conduction disturbances in aging human atrial bundles: experimental and model study. *Heart Rhythm.* 4:175–185.

10. Hubbard, M. L., W. Ying, and C. S. Henriquez. 2007. Effect of gap junction distribution on impulse propagation in a monolayer of myocytes: a model study. *Europace.* 9:vi20–vi28.

11. Spach, M. S., J. F. Heidlage, P. C. Dolber, and R. C. Barr. 2000. Electrophysiological effects of remodeling cardiac gap junctions and cell size: experimental and model studies of normal cardiac growth. *Circ. Res.* 86:302–311.

12. Hoyt, R. H., M. L. Cohen, and J. E. Saffitz. 1989. Distribution and three-dimensional structure of intercellular junctions in canine myocardium. *Circ. Res.* 64:563–574.

13. Saffitz, J. E., H. L. Kanter, K. G. Green, T. K. Tolley, and B. C. Bayer. 1994. Tissue-specific determinants of anisotropic conduction velocity in canine atrial and ventricular myocardium. *Circ. Res.* 74:1065–1070.

14. Lue, W. M., and P. A. Boyden. 1992. Abnormal electrical properties of myocytes from chronically infarcted canine heart. Alterations in Vmax and the transient outward current. *Circulation.* 85:1175–1188.

15. Page, E., and L. P. McCallister. 1973. Quantitative electron microscopic description of heart muscle cells: application to normal, hypertrophied, and thyroxin-stained hearts. *Am. J. Cardiol.* 31:172–181.

16. Cabo, C., and P. A. Boyden. 2003. Electrical remodeling of the epicardial border zone in the canine infarcted heart: a computational analysis. *Am. J. Physiol. Heart Circ. Physiol.* 284:H372–H384.

17. Cabo, C., and P. A. Boyden. 2006. Heterogeneous gap junction remodeling stabilizes reentrant circuits in the epicardial border zone of the healing canine infarct: a computational study. *Am. J. Physiol. Heart Circ. Physiol.* 291:H2606–H2616.

18. Joyner, R. W., F. Ramon, and J. W. Moore. 1975. Simulation of action potential propagation in an inhomogeneous sheet of coupled excitable cells. *Circ. Res.* 36:654–661.

19. Spach, M. S., J. F. Heidlage, P. C. Dolber, and R. C. Barr. 1998. Extracellular discontinuities in cardiac muscle: evidence for capillary effects on the action potential foot. *Circ. Res.* 83:1144–1164.

20. Henriquez, C. S. 1993. Simulating the electrical behavior of cardiac tissue using the bidomain model. *Crit. Rev. Biomed. Eng.* 21:1–77.

21. Roberts, D. E., and A. M. Scher. 1982. Effect of tissue anisotropy on extracellular potential fields in canine myocardium in situ. *Circ. Res.* 50:342–351.

22. Fleischhauer, J., L. Lehmann, and A. G. Kleber. 1995. Electrical resistances of interstitial and microvascular space as determinants of the extracellular electrical field and velocity of propagation in ventricular myocardium. *Circulation.* 92:587–594.

23. Hall, J. E. 1975. Access resistance of a small circular pore. *J. Gen. Physiol.* 66:531–532.

24. Wilders, R., and H. J. Jongsma. 1992. Limitations of the dual voltage clamp method in assaying conductance and kinetics of gap junction channels. *Biophys. J.* 63:942–953.

25. Aguilella-Arzo, M., V. M. Aguilella, and R. S. Eisenberg. 2005. Computing numerically the access resistance of a pore. *Eur. Biophys. J.* 34:314–322.

26. Kleber, A. G., and C. B. Riegger. 1987. Electrical constants of arterially perfused rabbit papillary muscle. *J. Physiol.* 385:307–324.

27. Gutstein, D. E., G. E. Morley, H. Tamaddon, D. Vaidya, M. D. Schneider, et al. 2001. Conduction slowing and sudden arrhythmic death in mice with cardiac-restricted inactivation of connexin43. *Circ. Res.* 88:333–339.

28. Yao, J. A., D. E. Gutstein, F. Liu, G. I. Fishman, and A. L. Wit. 2003. Cell coupling between ventricular myocyte pairs from connexin43-deficient murine hearts. *Circ. Res.* 93:736–743.

29. Plonsey, R., and R. C. Barr. 1986. A critique of impedance measurements in cardiac tissue. *Ann. Biomed. Eng.* 14:307–322.

30. Barr, R. C., and R. Plonsey. 2003. Electrode systems for measuring cardiac impedance using optical transmembrane potential sensors and interstitial electrodes-theoretical design. *IEEE Trans. Biomed. Eng.* 50:925–934.

31. Pollard, A. E., and R. C. Barr. 2006. Cardiac microimpedance measurement in two-dimensional models using multisite interstitial stimulation. *Am. J. Physiol. Heart Circ. Physiol.* 290:H1976–H1987.

32. De Bakker, J. M., F. J. van Capelle, M. J. Janse, S. Tasseron, N. Vermeulen, et al. 1993. Slow conduction in the infarcted human heart. 'Zigzag' course of activation. *Circulation.* 88:915–926.

33. Ursell, P. C., P. I. Gardner, A. Albala, J. J. Fenoglio, Jr., and A. L. Wit. 1985. Structural and eletrophysiological changes in the epicardial border zone of the infarcted heart. *Circ. Res.* 56:436–451.

34. Kleber, A. G., C. B. Riegger, and M. J. Janse. 1987. Electrical uncoupling and increase of extracellular resistance after induction of ischemia in isolated, arterially perfused rabbit papillary muscle. *Circ. Res.* 61:271–279.